EurJIC
European Journal of Inorganic Chemistry

Research Article
doi.org/10.1002/ejic.202400526

Chemistry Europe
European Chemical Societies Publishing

www.eurjic.org

Atomically Precise Rhodium-Gold Carbonyl Nanoclusters: In-Depth Synthesis and Multivalence Investigation of $[Rh_{16}Au_6(CO)_{36}]^{6-}$, and its Correlation with $[Rh_{10}Au(CO)_{26}]^{3-}$

Silvia Ruggieri,[a, b] Guido Bussoli,[a] Marco Bortoluzzi,[c] Cristiana Cesari,[a] Tiziana Funaioli,[d] Stefano Zacchini,[a] Maria Carmela Iapalucci,*[a] and Cristina Femoni*[a]

The synthesis of the previously-reported atomically-precise $[Rh_{16}Au_6(CO)_{36}]^{6-}$ (**1**) nanocluster has been optimized by screening different reaction variables like solvent, stoichiometric ratio, counterion and atmosphere. Its multivalence properties have also been studied by means of electrochemical and spectroelectrochemical techniques; the results pointed out a remarkable electron-sponge behaviour, as under such experimental conditions **1** is capable to release one electron and accept up to four more, while retaining its molecular structure. This scarce structural variation has been confirmed through DFT calculations on those species whose redox processes showed the maximum reversibility, namely $[Rh_{16}Au_6(CO)_{36}]^{7-}$ and $[Rh_{16}Au_6(CO)_{36}]^{5-}$. Moreover, we report herein the isolation and characterization of the new $[Rh_{10}Au(CO)_{26}]^{3-}$ (**2**) nanocluster, which represents one of the major fallouts of the synthetic pathway investigation of **1**. Finally, we disclosed the existence of further species that, from preliminary results, appear to be new large atomically-precise Rh–Au nanoclusters, which will be the subject of future investigations. Cluster **2** has been identified via single-crystal X-ray diffraction analysis, and the characterization of both clusters **1** and **2** completed by infrared (IR) spectroscopy and Electrospray Ionization Mass Spectrometry (ESI-MS).

Introduction

Molecular compounds containing gold atoms stabilized by different types of ligands have been known and studied for decades, both because of gold's unique optical,[1] biologic[2] and catalytic[3] properties, and also for fundamental research.[4] More recently, a considerable attention has been devoted to atomically-precise gold nanoclusters,[5] which have the peculiarity of possessing nanosized dimension and, at the same time, a structure known at a molecular level disclosed by single-crystal X-ray diffraction analyses.

The "atomically-precise" adjective is perfectly suitable also to metal nanoclusters stabilized by carbonyl ligands,[6] which had been known for decades beforehand.[7] In terms of Au-containing carbonyl nanoclusters, the ability of gold towards π-backdonation is knowingly weak, at least when compared to that of other *d*-block metals, therefore the CO shell is preferably coordinated to the latter. It is, however, worth mentioning that Au(I) carbonyl complexes have been reported in the literature,[8] and their bonding features deeply studied.[9]

Most heterometallic atomically-precise carbonyl nanoclusters containing gold are synthesized from the reaction of a preformed carbonyl compound with Au(I) or Au(III) complexes.[10] Whenever the ligand coordinated to the gold cation is fairly strongly bonded, like in the case of phosphine ligands (herein generally referred as L), the resulting products are mainly heterometallic species surface-decorated by [AuL] fragments (Figure 1).[11]

If, conversely, Au(I) or Au(III) cations are coordinated to more labile ligands, for instance halides, then their reaction with a preformed carbonyl precursor is likely to result in the formation of heterometallic clusters with naked Au atoms inserted inside the metal cage (Figure 2).[12] It is important to underline, however, that these are rules of thumb and, in some cases, clusters with interstitial gold atoms may be obtained by using $Au(PPh_3)Cl$ as initial reactant.[12a]

The *state of the art* for heterometallic carbonyl clusters and nanoclusters containing Au atoms as part of their metal skeleton indicates that they are mostly Ni-,[12a] Pd-,[12b] and Fe[12c] based. Their preparation commonly exploits the well-known redox condensation method,[13] which generally consists in reacting a pre-formed carbonyl cluster anion of one metal type

[a] S. Ruggieri, G. Bussoli, C. Cesari, S. Zacchini, M. C. Iapalucci, C. Femoni
Department of Industrial Chemistry "Toso Montanari", University of Bologna, Via Gobetti 85, 40129 Bologna, Italy
E-mail: maria.iapalucci@unibo.it
cristina.femoni@unibo.it

[b] S. Ruggieri
Laboratory of Luminescent Materials, Department of Biotechnology, University of Verona and INSTM, UdR Verona, Strada Le Grazie 15, 37134 Verona, Italy

[c] M. Bortoluzzi
Department of Molecular Sciences and Nanosystems, Ca' Foscari University of Venice, Via Torino 155, 30170 Mestre (VE), Italy

[d] T. Funaioli
Department of Chemistry and Industrial Chemistry, University of Pisa, Via Moruzzi 13, 56124 Pisa, Italy

Supporting information for this article is available on the WWW under https://doi.org/10.1002/ejic.202400526

Research Article
doi.org/10.1002/ejic.202400526

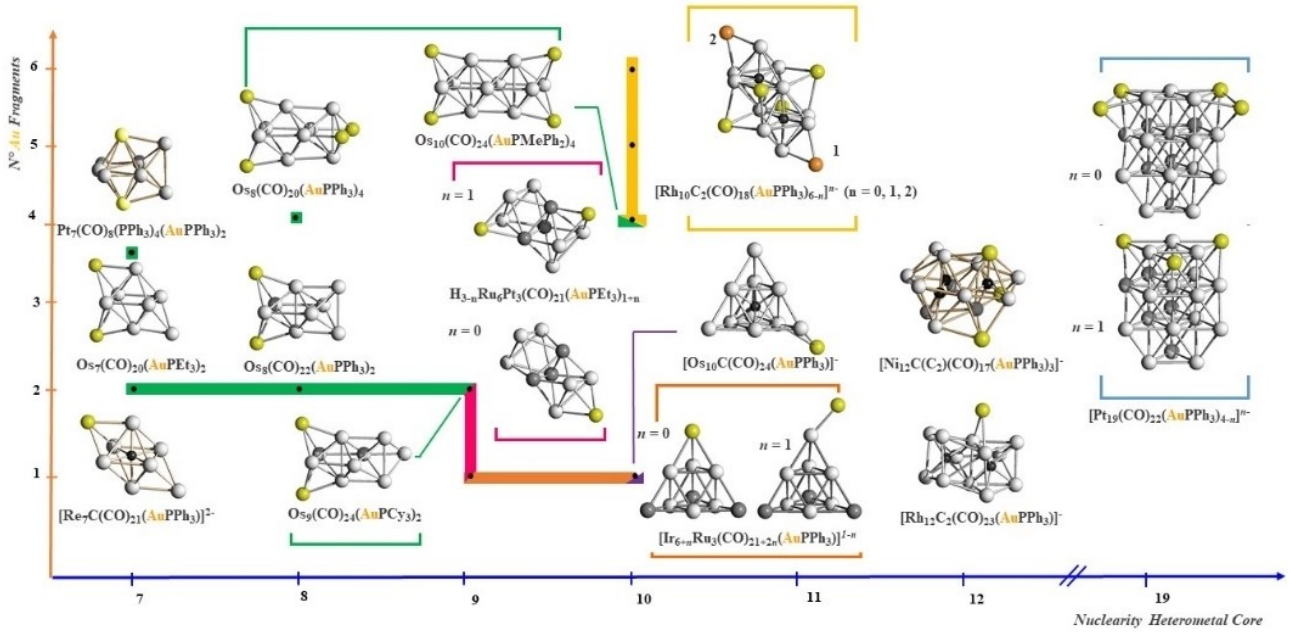

Figure 1. Overview of some selected examples of transition metal carbonyl clusters surface-decorated by [AuL] fragments (L = phosphine ligand). Yellow spheres indicate gold. Carbonyl and L ligands have been omitted for sake of clarity. (*Reproduced with permission of Elsevier from* I. Ciabatti, C. Femoni, M. C. Iapalucci, S. Ruggieri, S. Zacchini, *Coord. Chem. Rev.* **2018**, *355*, 27–38).[10]

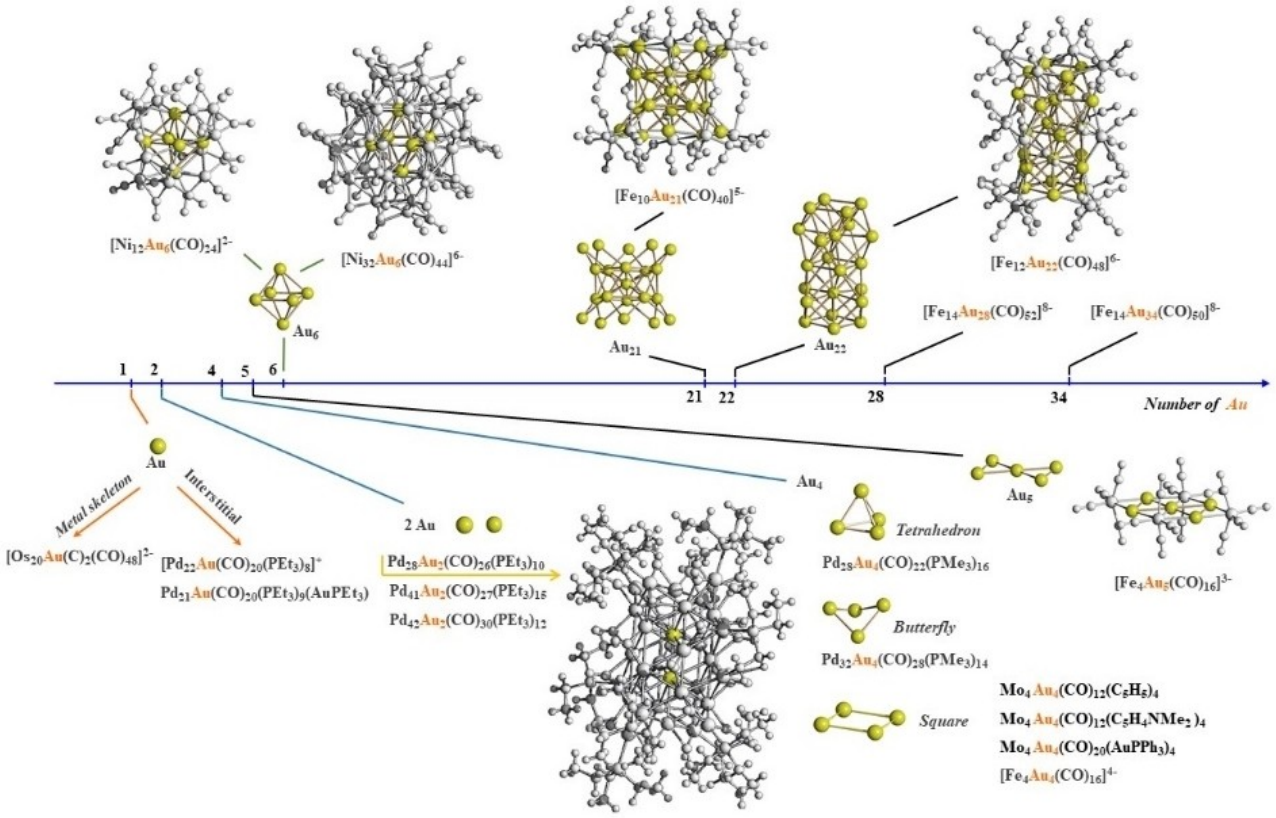

Figure 2. Graphical overview of carbonyl clusters containing Au atoms embedded in the metal framework. Yellow spheres indicate gold (*Reproduced with permission of Elsevier from* I. Ciabatti, C. Femoni, M. C. Iapalucci, S. Ruggieri, S. Zacchini, *Coord. Chem. Rev.* **2018**, *355*, 27–38).[10]

and a complex of a different metal cation, so to give heterometallic species composed of CO-stabilized compounds with the metals in different oxidation states with respect to the starting ones. The advantage of such method lies on the fact

Research Article
doi.org/10.1002/ejic.202400526

that, being the driving force of the reaction mainly due to the reactants' different reduction potentials, it can be carried out under mild conditions of temperature and pressure. It is also a versatile method that can be exploited to prepare large carbonyl nanoclusters with combinations of different metals[14] and post-transition elements.[15]

Considering the lack of Rh–Au species, and in view of our expertise in the synthesis and characterization of atomically-precise carbonyl nanoclusters, we previously carried out a sort of *proof-of-concept* study investigating the possibility of preparing Rh–Au compounds, and preliminarily reported the obtaining of a unique heterometallic species, namely $[Rh_{16}Au_6(CO)_{36}]^{6-}$ (**1**).[16] In the present paper we describe its optimized synthesis that also allowed us to disclose the existence of another new species, $[Rh_{10}Au(CO)_{26}]^{3-}$ (**2**), unambiguously identified via single-crystal X-ray diffraction (SC-XRD) analysis and characterized via infrared (IR) spectroscopy and Electrospray Ionization Mass Spectrometry (ESI-MS). Moreover, we completed the characterization of $[Rh_{16}Au_6(CO)_{36}]^{6-}$ and analysed its electron-sponge behaviour through electrochemical and spectroelectrochemical experiments. The results indicate that $[Rh_{16}Au_6(CO)_{36}]^{n-}$ can give rise to five long-lived species in the time scale of the spectroelectrochemical experiments (n = 5, 6, 7, 9, 10), all of which could be brought back to the parent cluster with a good degree of reversibility. Evidence of a cluster with n = 8 was also found, albeit always in co-existence with its immediate closed congeners. The stationary points of the two species presenting the best reversibility, namely the paramagnetic $[Rh_{16}Au_6(CO)_{36}]^{7-}$ and $[Rh_{16}Au_6(CO)_{36}]^{5-}$ deriving from the first reduction and oxidation process of the parent cluster, respectively, have been obtained by theoretical DFT calculations and compared with the ones of the hexaanion, confirming that the redox processes cause very scarce variations of the cluster structure. Ultimately, over the course of our investigation we disclosed the existence of further species that, from preliminary structural and spectroscopic results, appear to be new atomically-precise Rh–Au carbonyl nanoclusters. They will be the subject of future studies.

Results and Discussion

Reactions Screening

A previous study of rhodium-gold bimetallic system had led to the isolation of the large atomically-precise $[Rh_{16}Au_6(CO)_{36}]^{6-}$ (**1**) nanocluster, which was obtained by a redox condensation process between the already known $[Rh_7(CO)_{16}]^{3-}$[17] and $[AuCl_4]^-$ carried out in a 1 : 0.75 ratio, respectively, under carbon monoxide atmosphere, at room temperature and using dimethylformamide (DMF) as solvent.[16] However, it was quite clear that a complex bimetallic system was yet to be analysed as other species could be detected, and the reaction selectivity appeared to be rather poor. Indeed, $[Rh_{16}Au_6(CO)_{36}]^{6-}$ could only be obtained in fairly low yield (around 20% based on Rh). Therefore, we decided to deepen the study of the reaction leading to **1** trying to optimize it and, also, to understand the influence of the employed solvent, the related solubility of reactants/products, the role of the stoichiometric ratio and of the atmosphere under which the reaction is carried out.

Over the past, the cluster precursor showed to be very effective in preparing large heterometallic carbonyl species,[18] therefore the reference reaction between $[Rh_7(CO)_{16}]^{3-}$ and $[AuCl_4]^-$ was maintained. However, it was systematically tested under both N_2 and CO, and in different solvents and stoichiometric ratios, as well as with different counterions so to increase and/or decrease the solubility of the reactants and products, which is a key parameter to ease their separation from the reaction mixture. More specifically, the relatively small dimension of $[Rh_7(CO)_{16}]^{3-}$ combined with its high negative charge make it well soluble in polar solvents like acetonitrile and DMF, but poorly soluble in less polar solvents like tetrahydrofuran (THF), and only partially soluble in acetone. It is important to underline that, nonetheless, some degree of polarity in the solvent is needed to dissolve charged clusters, whereas neutral ones can easily be dissolved in apolar media. Like in most salts, the $[Rh_7(CO)_{16}]^{3-}$ solubility can be significantly tuned by employing tetraalkylammonium counterions with different length of the alkyl chains, taking into consideration that the longer the chain, the higher the solubility. The same principle applies to all clusters, including the obtained ones. The organic cations screened in this study were tetramethylammonium (TMA^+), tetraethylammonium (TEA^+), tetrapropylammonium (TPA^+), and tetrabutylammonium (TBA^+). The bulkier tribenzylmethylammonium ($TBMA^+$) was also exploited, but to ease cluster crystallization. To be sure to work in homogeneous conditions, either acetonitrile or DMF were employed, as they are able to dissolve large nanoclusters even with short-alkyl chain ammonium counterions. If, however, heterogenous conditions were desired, for instance to enhance separation of the formed products by their precipitation in the reaction medium, then THF was used. In such case, the counterion of choice had to be TBA^+, the only one able to solubilize $[Rh_7(CO)_{16}]^{3-}$.

All reactions' pathways were monitored via IR spectroscopy, and the work-up was carried out after 24 hours. When working in homogeneous conditions, when both the reactants and products were fully soluble, the final mixture was dried under vacuum, the solid washed with water and ethanol to eliminate tetraalkylammonium salts and possible Rh(I) complexes, respectively, dried again and then subsequently treated with solvents of increasing polarity (THF, acetone, acetonitrile), to separate and isolate the different products of increasing nuclearity and negative charge. The only exception to this procedure was when using DMF as solvent: in this case, due to its high boiling point, the product mixture was not dried under vacuum but recovered by precipitation with a saturated aqueous solution of the desired ammonium halide. When working in heterogeneous conditions, the formed precipitate at the end of the reaction was filtered off and treated separately from the mother solution, following the aforementioned procedure.

The first set of reactions was conducted under N_2 atmosphere. However, regardless of the employed counterion, solvent and stoichiometric ratio, all tests led to the formation of only

Research Article
doi.org/10.1002/ejic.202400526

homometallic rhodium clusters, more specifically the known $[Rh_{11}(CO)_{23}]^{3-}$[19] and $[Rh_{12}(CO)_{30}]^{2-}$,[20] which are both expected oxidation products of $[Rh_7(CO)_{16}]^{3-}$ that can be brought about by different oxidizing agents.[21] In the present case, the oxidation was brought about by Au(III), which in turn was reduced to metallic gold. The formation of $[Rh(CO)_2Cl_2]^-$ was also detected, again a common fallout in such environment. No heterometallic species were identified during this first screening under N_2.

Considered the above results, we focused our attention on the reactions carried out under carbon monoxide atmosphere. We employed $[Rh_7(CO)_{16}]^{3-}$ and $[AuCl_4]^-$ starting with a 1:0.5 ratio, respectively, with TEA^+ as unique counterion to allow their full solubility in acetonitrile, as well as that of the obtained products. However, in such solvent the reaction confirmed to be poorly selective, as we obtained the targeted cluster **1** but in a very low yield and in mixture with other homometallic and heterometallic products. Among the former we identified the $[Rh(CO)_2Cl_2]^-$ complex (extracted in ethanol), and the already known $[Rh_5(CO)_{15}]^-$[22] (extracted in THF). The extraction in acetone evidenced the presence of an unknown large and possibly homometallic Rh cluster, which is currently under investigation (here referred as cluster **A**); the final acetonitrile fraction isolated what, from preliminary results, seems to be another new nanocluster, but this time of heterometallic nature (here referred as cluster **B**), and in mixture with cluster **1**.

We repeated the same reaction in a 1:1 ratio but it was clear that even this did not impart any significant selectivity. The main differences with the precedent stoichiometry were the absence of the presumed homometallic species (cluster **A**) and the detection of another unknown product in the acetone extraction (later identified as cluster **2**), while the acetonitrile fraction still extracted cluster **1**, but in a lower amount. The increase of Au(III) beyond 1 equivalent led to yet another new species (here referred as cluster **C**), therefore we decided to set this set of reaction aside for future studies.

We moved on and decided to work under heterogeneous conditions, always under carbon monoxide atmosphere. In order to do so, we searched for the best combination of solvent and ammonium cation that would solubilize the reactants but not all the products, at least not the highly charged ones, which are generally those with the higher nuclearity. After several attempts the optimised conditions were to carry out the reaction in THF using TBA^+ as counterion for the cluster precursor and TEA^+ for the Au(III) complex, and to use 1 equivalent of $[AuCl_4]^-$ per equivalent of $[Rh_7(CO)_{16}]^{3-}$. After leaving the final mixture under stirring overnight, the formed precipitate was filtered to separate it from the solution, which evidenced the presence of the expected $[Rh(CO)_2Cl_2]^-$ and $[Rh_5(CO)_{15}]^-$ species. As for the precipitate, we added an extra-step in the procedure and started the extraction with dichloromethane, which solubilized traces of an unknown species that we were not able to identify (later recognized as cluster **2**). Then the residue was firstly extracted in acetone but, due to partial solubility, subsequently solubilized in acetonitrile, and the IR spectrum indicated the sole presence of the desired $[Rh_{16}Au_6(CO)_{36}]^{6-}$. Its identity in its TEA^+ salt was confirmed by SC-XRD analysis performed on the crystals obtained after layering a small amount of hexane and di-isopropyl ether on to the acetonitrile solution. Remarkably, when the reaction was repeated but using TBA^+ for both $[Rh_7(CO)_{16}]^{3-}$ and $[AuCl_4]^-$, no precipitate was formed and cluster **1** was only found in traces in the final mixture.

All above experimental evidence led us to conclude that, under CO atmosphere, **1** is the first heterometallic product that originates from the reaction of $[Rh_7(CO)_{16}]^{3-}$ with $[AuCl_4]^-$, but it can undergo subsequent reactions leading to different clusters. Such occurrence is very likely if **1** is soluble in the reaction media, while if it precipitates right after its formation, then it remains stable. In order to maximize the formation of **1**, therefore, it is necessary to carry out the reaction under heterogenous conditions, that is in THF using $[Rh_7(CO)_{16}]^{3-}$ in its TBA^+ salt but ensuring that some TEA^+ is present to allow the precipitation of **1**$[TEA]_6$, insoluble in such solvent. Any other counterion combined with TBA^+, for instance TMA^+ and TPA^+, did not allow selective precipitation of **1**.

The previously reported synthesis of cluster **1** had been carried out in DMF,[16] therefore under homogeneous conditions; indeed, in agreement with the above conclusions, the obtained yield was significantly lower than that obtained under the heterogeneous conditions ensured by THF (around 20% based on Rh, against a 35% yield achieved with the new optimized synthesis).

Nevertheless, to continue our reaction screening, we replicated the original procedure in DMF but, with hindsight, we increased the amount of Au(III) complex up to 1 equivalent, considering the good results obtained with the reaction carried out in THF.

As previously mentioned, the work-up on the final mixture required its preliminary precipitation by adding dropwise an aqueous solution of the desired tetraalkylammonium salt, in our case TEACl. After having washed with water the precipitated solid mixture, the first two extractions in ethanol and THF solubilized $[Rh_5(CO)_{15}]^-$, while the one in acetone showed an unknown IR spectrum, the same observed in the acetone and dichloromethane fractions in the reactions carried out in acetonitrile and THF under CO, respectively. This solution was layered with hexane in the attempt to obtain suitable crystals for the SC-XRD analysis. Having failed this, we performed a metathesis with a bulkier counterion, $TBMA^+$, and this time we succeeded in obtaining black needle-shaped crystals of a new species, $[Rh_{10}Au(CO)_{26}]^{3-}$ (**2**). Its molecular structure is described in detail in the specific section. The final extraction in acetonitrile evidenced only traces of cluster **1**.

Our investigation in DMF continued by varying the Rh_7:Au(III) ratio, going from 1:0.75 to 1:1.5 and up to 1:2. When working in defect of Au(III), the reaction loses selectivity in $[Rh_{10}Au(CO)_{26}]^{3-}$ with respect to the reaction carried out with a 1:1 ratio. On the other hand, when the amount of Au(III) is taken to 1.5 equivalents with respect to the Rh cluster precursor, no traces of $[Rh_{16}Au_6(CO)_{36}]^{6-}$ are detected, whereas cluster **2** was found in mixture with another new species (cluster **C**, the same obtained in the acetonitrile reaction with

Research Article
doi.org/10.1002/ejic.202400526

an excess of oxidant) whose formation is maximized when working with 2 equivalents of Au(III).

These results confirmed the hypothesis that cluster **1** is the first heterometallic cluster obtainable from the reaction of $[Rh_7(CO)_{16}]^{3-}$ with $[AuCl_4]^-$ carried out under CO atmosphere, and that its oxidation to cluster **2** is caused by an excess of Au(III) in the reaction medium. This is also in line with the tested stochiometric ratios. The suitable combination of counterion and solvent allows to either keep cluster **1** in solution, so once formed it can further react with Au(III) undergoing a subsequent reaction, or to make it precipitate in the solid state to prevent it from doing so. Cluster **1** can therefore yield to cluster **2** in the former case, but from experimental evidence it seems that cluster **2** cannot be reconverted into cluster **1**.

Another conclusion that we can draw is that, although both DMF and acetonitrile allowed to work under homogeneous conditions, the different work-up may have an influence on the reaction path. In fact, the 1:1 ratio was more selective towards cluster **2** when the reaction was carried out in DMF with respect to the one in acetonitrile, and this could be due to the fact that in the latter case, as the mother solution is dried in vacuum, an increase of concentration occurs and this may lead to undesired side reactions.

The last tested solvent was acetone, and TPA^+ was used as counterion for $[Rh_7(CO)_{16}]^{3-}$, while for Au(III) both TPA^+ and TEA^+ were tried. Another new species, albeit in traces, was detected when mixed cations were employed (here referred as cluster **D**), most likely isolated thanks to the different solubility imparted by the TPA^+ counterion, but these results will be reported elsewhere.

Scheme 1 summarizes the key points of the reactions screening under CO, highlighting the major outcomes in terms or heterometallic carbonyl clusters. The unknown clusters (**A**–**D**) have been identified through IR spectroscopy and, in some cases, preliminary X-ray analyses that provided information on their metal frameworks.

Characterization

After having found a more selective synthesis for $[Rh_{16}Au_6(CO)_{36}]^{6-}$ (**1**) by working under heterogeneous conditions, we completed its characterization via IR and ESI-MS registered on selected crystals dissolved in acetonitrile (details are reported in the Supporting Information section in Figures S1a–c and in Table S1a). As for the mass spectrometry, we were able to prevent the cluster fragmentation under the experimental conditions by working at lower cone voltage in the ionization chamber than the one used when we firstly reported the obtaining of **1**. In the negative-ion spectrum it is possible to see the molecular ion with a maximum of 30 carbonyl ligands out of its original 36, plus other peaks corresponding to subsequent losses of one ligand at a time, down to a minimum of 22. This occurrence is always happening during the ESI-MS analyses, and it is indeed a desired feature as the CO loss enables the correct assignment of *z* in the mass spectra. In fact, the cluster charge resulting from the analysis is hardly ever the original one, and generally all signals corre-

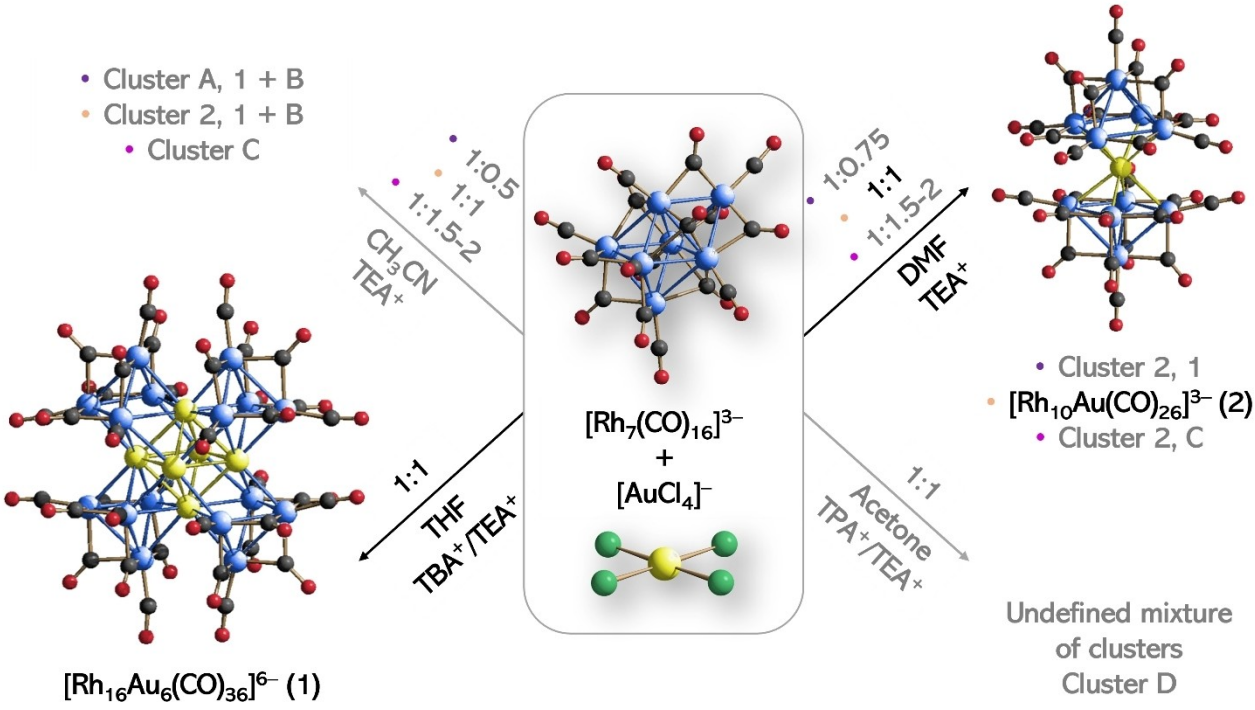

Scheme 1. Summary of the reactions screening carried out under CO using various solvents, stoichiometric ratios and counterions. Only the main obtained products in terms of metal clusters are indicated. In grey the reactions that will be the subject of further investigation.

Research Article
doi.org/10.1002/ejic.202400526

spond to ions with $z=2$ and 3 in the negative region. This is, again, a very common feature in the carbonyl cluster chemistry, especially those with high nuclearity. Notably, Rh-based clusters are actually more robust than others thank to their high Rh–Rh and Rh-CO bond strengths.[23]

We also investigated the electronic properties of **1** via electrochemical and spectroelectrochemical experiments, the details of which are described in the dedicated section, to assess its multivalence behaviour in analogy with what observed in the past for species of similar nuclearity.

As for the new bimetallic $[Rh_{10}Au(CO)_{26}]^{3-}$ (**2**), its IR and ESI-MS spectra are reported in the Supporting Information (Figure S2a–c and Table S2a), as well as its crystallographic data (Table S2b) and selected bond lengths (Table S2c) derived from its SC-XRD characterization. In the negative region of the ESI-MS spectrum it is worth noting that the cluster is partially stable under the experimental conditions, as we can also see signals attributable to a $\{Rh_5Au(CO)_{11}\}^{2-}$ fragment, together with some derived from the molecular ion ($z=2$ and 3) with a maximum of 21 carbonyl ligands out of 26, with and without the counterion.

Molecular Structure of $[Rh_{10}Au(CO)_{26}][TBMA]_3$ (2)[24]

Cluster **2** in its $TBMA^+$ salt crystallized in a monoclinic system, and the unit cell contains four cluster units and twelve $TBMA^+$ cations. The packing in the solid state alternates cluster anions and ammonium cations in an ionic fashion. The molecular structure of **2** is illustrated in Figure 3, and it consists of two Rh_5Au octahedra sharing the Au atom, slightly tilted with respect to each other. Another way of describing the metal skeleton is considering two $\{Rh_5(CO)_{13}\}$ cluster moieties joint through a gold atom. This arrangement resembles that of $[Ni_{12}Au(CO)_{24}]^{3-}$,[25] where the gold atom connects two $[Ni_6(CO)_{12}]^{2-}$ clusters. Notably, the $\{Rh_5(CO)_{13}\}$ units differ from the known $[Rh_5(CO)_{15}]^-$ as the latter possesses a trigonal pyramidal geometry, and not a square pyramidal one. The literature reports a few further examples where two cluster units are sandwiched between naked Au(I)[10] or, more generally, *d*10 ions, for instance $[\{Co_5C(CO)_{12}\}_2Au]^-$,[26] $[\{Pt_3(CO)_3(PPh_3)_3\}_2Au]^+$,[27] $[\{Pt_3(CO)_3(PMe_3)_4\}_2Au]^+$,[28] $[\{HOs_3(CO)_{10}\}_2Au]^-$,[29] $[\{Fe_2(CO)_8\}_2Au]^-$[30] in the former case, $[Hg\{RuCo_3(CO)_{12}\}_2]$,[31] $[\{Ru_3(CO)_{11}\}_2Au]^{2-}$[32] and $\{[AgRu_6C(CO)_{16}][PPN]\}_\infty$[33] in the latter.

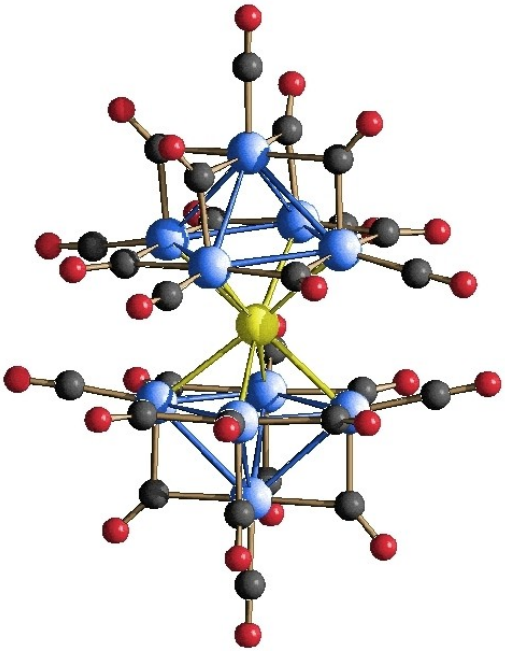

Figure 3. Molecular structure of $[Rh_{10}Au(CO)_{26}]^{3-}$. Rhodium atoms are depicted in blue, gold atoms in yellow, carbon atoms in grey and oxygen atoms in red.

The ligand shell of **2** is composed of 26 carbonyl groups, of which 10 terminally bonded to each Rh atom, and the remaining 16 bridging all the Rh–Rh edges.

The octahedral motif found in **2** is also encountered in **1**. Indeed, the metal framework of $[Rh_{16}Au_6(CO)_{36}]^{6-}$ consists of an Au_6 octahedron surrounded by sixteen Rh atoms arranged in a way so to compose four Rh_4Au_2 octahedra, each built on the edge of the squared base of the inner golden polyhedron. For sake of comparison, the metal skeletons of cluster **1** and **2** highlighting the various octahedra are illustrated in Figure 4.

Remarkably, the same octahedral-based architecture can be observed in the large atomically-precise $[Ni_{32}Au_6(CO)_{44}]^{6-}$ nanocluster[12a] whose $Ni_{24}Au_6$ inner core is composed of an Au_6 octahedron onto which eight more octahedra are built, more specifically two Ni_3Au_3 on opposite sides of the golden polyhedron, and six Ni_4Au_2 ones (Figure 5).

The average Rh–Rh bond lengths in cluster **2** is 2.9195 Å, while the Rh–Au ones have average of 2.7419 Å. The latter value is perfectly in line with that found in cluster **1** (2.797 Å), while the former is slightly longer, being the Rh–Rh average bond length in cluster **1** equal to 2.841 Å. For sake of comparison, in $[Ni_{32}Au_6(CO)_{44}]^{6-}$ the Au–Au bond lengths have an average of 2.875 Å. The full list of metal-metal bond for $[Rh_{10}Au(CO)_{26}]^{3-}$ is reported in Table S2c.

Electrochemistry and Spectroelectrochemistry of $[Rh_{16}Au_6(CO)_{36}][TEA]_6$

The redox properties of $[Rh_{16}Au_6(CO)_{36}][TEA]_6$ have been studied by cyclic voltammetry (CV) at a glassy carbon (GC) working electrode (WE), in CH_3CN solutions containing $[TBA][PF_6]$ (0.1 mol dm^{-3}) as supporting electrolyte, and under CO atmosphere. This analysis has been integrated by *in situ* infrared spectroelectrochemical (IR SEC) measurements of a CH_3CN/$[TBA][PF_6]$ solution, in an OTTLE cell,[34] under CO atmosphere, resolution 4 cm^{-1}. In the case of the CV analysis, in the scanned potential range from +0.3 to −2.0 V cluster **1** exhibits a rich redox activity; in fact, as shown in Figure 6, it undergoes four oxidations and four reduction processes. The same number of electrons appears to be involved in the oxidation processes and in the first two reduction ones, with features of chemical reversibility in the cyclic voltammetry time-scale. The peak-to-peak separations measured at 0.2 V s^{-1} are around 80 mV in the

Research Article
doi.org/10.1002/ejic.202400526

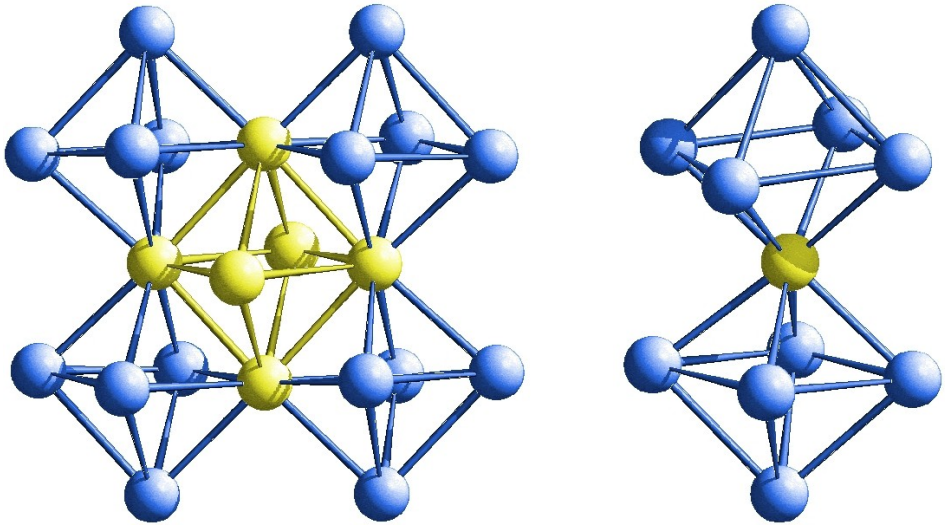

Figure 4. Metal framework of $[Rh_{16}Au_6(CO)_{36}]^{6-}$ (left) and $[Rh_{10}Au(CO)_{26}]^{3-}$ (right) with highlighted the Au_6, Rh_4Au_2 (cluster **1**) and Rh_5Au (cluster **2**) octahedra. Rh atoms are in blue, Au atoms in yellow.

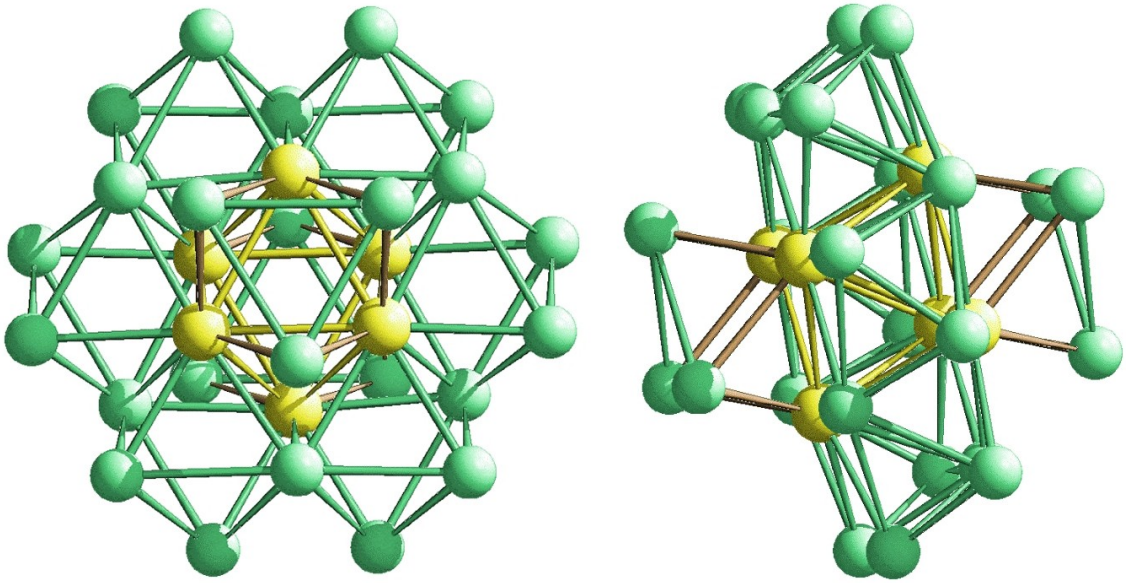

Figure 5. Front and side view of the *$Ni_{24}Au_6$* inner architecture of the $[Ni_{32}Au_6(CO)_{44}]^{6-}$ nanocluster. The core is composed of one interstitial Au_6 octahedron (defined by yellow bonds), two face-sharing Ni_3Au_3 octahedra (defined with brown bonds) and six edge-sharing Ni_4Au_2 octahedra (defined by green bonds). Au atoms are depicted in yellow, Ni atoms in green.

four oxidation processes, and around 100 mV in the two reduction ones. The two further reduction processes at −1.71 and −1.87 V, respectively, are ill-defined and complicated by relatively fast chemical reactions.

Formal electrode potentials for the observed electron transfers are reported in Table 1.

The results obtained from the CV experiments were confirmed by IR SEC measurements, always carried out under CO atmosphere. The IR spectra were recorded every 60 seconds during a slow potential scan (1 mV s^{-1}) between −0.5 and −2.0 V. The complete sequence, reported in Figure S1d, shows a shift of the CO stretching frequencies of the parent cluster (ν_{CO} 2007, 1982 and 1803 cm^{-1}) towards lower values upon

Table 1. Formal electrode potentials (V *vs* Ag/AgCl) for the redox processes exhibited by $[Rh_{16}Au_6(CO)_{36}]^{6-}$ in CH_3CN/[TBA][PF_6] solution under CO atmosphere.

Reduction processes			
E°_1	E°_2	E°_3	E°_4
−1.87[a]	−1.71[a]	−1.44	−1.20
Oxidation processes			
E°_5	E°_6	E°_7	E°_8
−0.62	−0.40	−0.13	+0.09

[a] Coupled to relatively fast chemical reactions.

Research Article
doi.org/10.1002/ejic.202400526

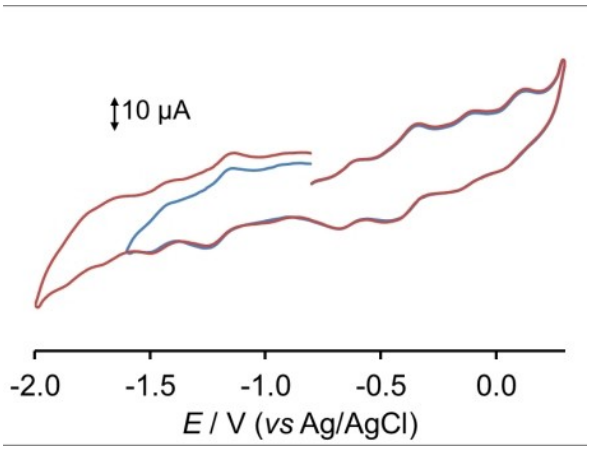

Figure 6. Cyclic voltammetric profiles recorded at a glassy carbon electrode in CH_3CN solution of $[Rh_{16}Au_6(CO)_{36}]^{6-}$ between −2.0 and +0.3 V (red line) or −1.6 and +0.3 V (blue line). [TBA][PF_6] (0.1 mol dm^{-3}) supporting electrolyte. Scan rate: 0.2 V s^{-1}.

reduction, as a result of the increased negative charge, and towards higher values upon oxidation.

The IR spectrum of the starting cluster was re-obtained in quantitative/high yields as the potential was reversed to the initial value, demonstrating a relatively high stability of the obtained redox states of the cluster also in the time-scale of the spectroelectrochemical experiments.

To assign the charge to the electrogenerated species we referred to the previously observed behaviour of other carbonyl nanoclusters,[35] where the shift values related to the stretching frequencies of terminal CO ligands are within a range of around 15–25 cm^{-1} per added/removed electron.

On such basis and considering the relative *i/E* profile curve and the maxima of the terminal and bridging CO stretching bands, the sequence of the recorded IR spectra was separated in four groups, each belonging to a different redox process (Figure 7).

The stability of each redox state was verified by the comparison between the initial spectrum of the cluster and the one obtained by reverting the scan potential after each step. In this way we could demonstrate that, at increasing potentials, only the product of the mono-oxidation $[Rh_{16}Au_6(CO)_{36}]^{5-}$ (Figure 7a, ν_{CO} 2024 and 1836 cm^{-1}) is fairly stable in the long time of the IR SEC experiment, since the starting cluster could be regenerated in very high yields (Figure S1e). Indeed, when the potential was increased above −0.5 V, the complete cluster decomposition was pointed out by the decrease of the IR absorptions of $[Rh_{16}Au_6(CO)_{36}]^{5-}$ and by the appearance of two carbonyl bands at 2120 and 2063 cm^{-1} (Figure S1f) due to the formation of the mononuclear cationic $[Rh(CO)_2(CH_3CN)_2]^+$ complex.[36]

The same full reversibility was observed for the first reduction process. In fact, when the WE potential was decreased from −0.8 to −1.4 V (Figure 7b) the shift of the stretching CO bands at 1989, 1965 and 1784 cm^{-1} was accompanied by a change of the band shape (relative intensity and width) of terminal CO stretching bands, but the starting

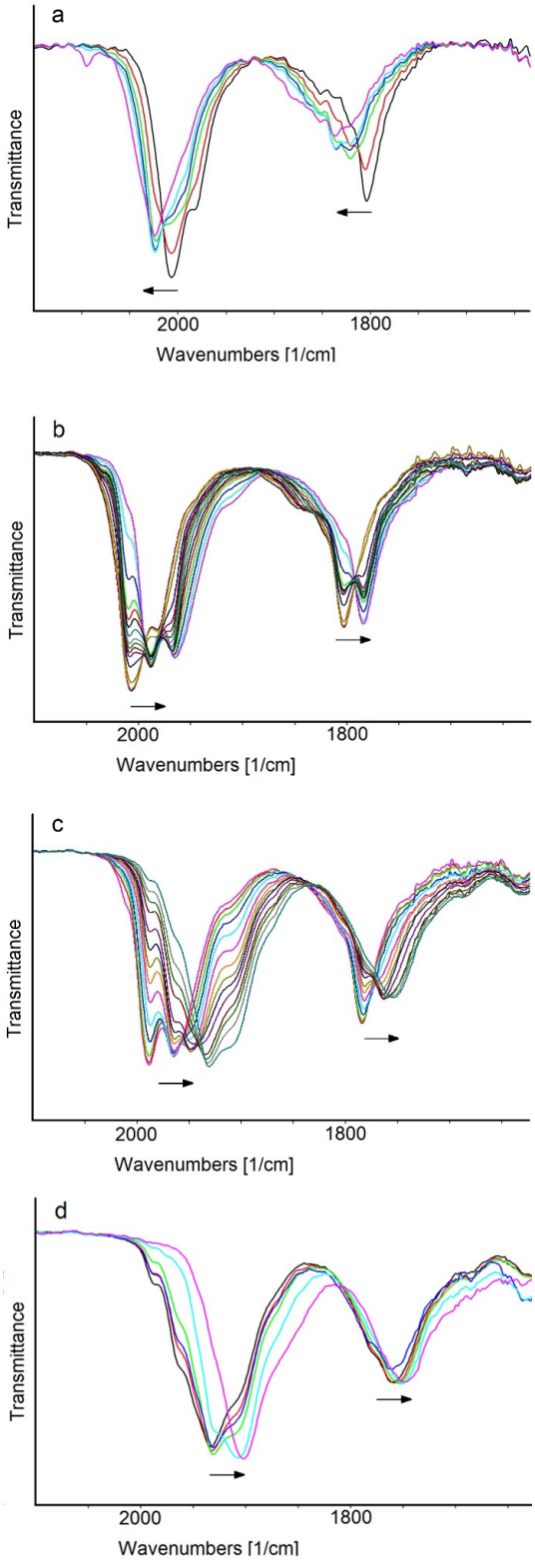

Figure 7. Infrared spectra of $[Rh_{16}Au_6(CO)_{36}]^{6-}$ in CH_3CN containing 0.1 mol dm^{-3} [TBA][PF_6], under CO atmosphere, recorded in an OTTLE cell during the progressive: a) increase of the WE potential from −0.8 to −0.5 V; b) decrease of the WE potential from −0.8 to −1.4 V; c) decrease of the WE potential from −1.4 to −1.7 V; d) decrease of the WE potential from −1.7 to −2.0 V. The solvent and supporting electrolyte absorptions have been subtracted. The left- and right-oriented arrows indicate oxidation and reduction processes, respectively.

Research Article
doi.org/10.1002/ejic.202400526

spectrum was completely restored in the backward oxidation (Figure S1g), pointing out the high stability of the radical anion $[Rh_{16}Au_6(CO)_{36}]^{7-}$.

In the IR spectra sequence recorded from −1.4 to −1.7 V (Figure 7c), the terminal CO-frequency downshift was in a range of around twice that observed for the above described redox changes (from 1989 and 1965 to 1931 cm^{-1}), indicating a two-electron step from $[Rh_{16}Au_6(CO)_{36}]^{7-}$ to $[Rh_{16}Au_6(CO)_{36}]^{9-}$. Moreover, in the complex pattern of intermediate spectra of Figure 7c, the presence of a transient additional charge state with n = 8 was suggested by one absorption maximum at 1949 cm^{-1}; this value was supported by a spectral deconvolution analysis of the middle spectrum of the sequence, whose details are reported in the Supporting Information (Figure S1h). The process reversibility was ascertained by the back-oxidation that restored $[Rh_{16}Au_6(CO)_{36}]^{6-}$ in fairly high yields (Figure S1i).

The WE potential could be further lowered to −2.0 V (Figure 7d) with only a moderate cluster decomposition, as demonstrated by the good recovery of $[Rh_{16}Au_6(CO)_{36}]^{6-}$ when the potential was brought back to −0.8 V (Figure S1l). The IR bands at 1907 and 1748 cm^{-1} were attributed to a relatively long-lived negative charge state −10. Extensive and fast cluster decomposition was observed for further potential decrease.

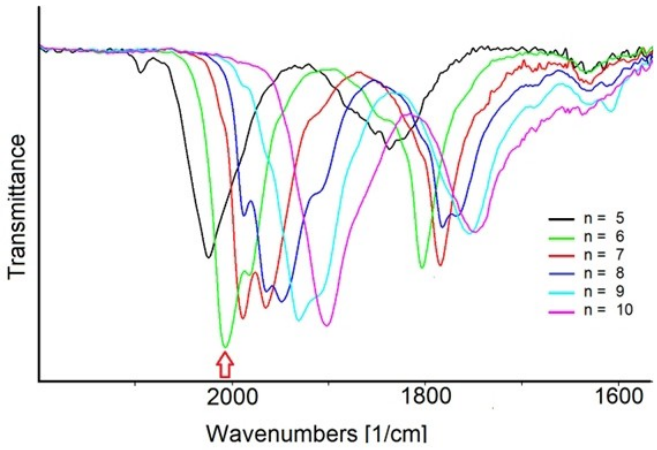

Figure 8. Selected infrared spectra of $[Rh_{16}Au_6(CO)_{36}]^{n-}$ as a function of the cluster charge n in CH_3CN containing 0.1 mol dm^{-3} [TBA][PF_6], under CO atmosphere. The absorptions of the solvent and supporting electrolyte have been subtracted. The red arrow indicates the initial spectrum.

Table 2. Infrared stretching frequencies (cm^{-1}) of terminal (ν^t_{CO}) and bridging (ν^b_{CO}) carbonyl groups for $[Rh_{16}Au_6(CO)_{36}]^{n-}$ in CH_3CN solution as a function of the cluster charge. The row in italic corresponds to the cluster charge deduced by spectral deconvolution.

Cluster charge n^-	ν^t_{CO} (cm^{-1})	ν^b_{CO} (cm^{-1})
n = 5	2024	1836
n = 6	2007, 1982	1803
n = 7	1989, 1965	1784
n = 8	*1965, 1949*	*1766*
n = 9	1931	1754
n = 10	1903	1748

Considering the combined results from the CV and the IR SEC experiments, we can conclude that four reversible oxidations and four reductions can be recognized in the voltammetric profile, but in the longer time scale of IR SEC only four long-lived different negative charge states of $[Rh_{16}Au_6(CO)_{36}]^{n-}$ were identified in addition to the initial one (n = 6) namely one obtained by oxidation (n = 5) and three by reduction, (n = 7, 9 and 10) (Figure 8). Evidence of one cluster with limited stability and charge −8 was obtained by an accurate analysis of the spectra of Figure 7c and a spectral deconvolution performed on the blue spectrum of Figure 8. Table 2 reports the IR stretching frequencies related to all the six differently charged $[Rh_{16}Au_6(CO)_{36}]^{n-}$ derivatives, as inferred by the SEC experiments and spectral deconvolution.

Theoretical Molecular Structures of $[Rh_{16}Au_6(CO)_{36}]^{n-}$ (n = 5, 6, 7): a Comparative Analysis

In light of the results obtained by the spectroelectrochemical experiments, we calculated the coordinates of the molecular structures for the two more stable and differently-charged $[Rh_{16}Au_6(CO)_{36}]^{n-}$ congeners adjacent to the starting one, more specifically those obtained by the first oxidation and the first reduction process of cluster **1**, namely $[Rh_{16}Au_6(CO)_{36}]^{5-}$ and $[Rh_{16}Au_6(CO)_{36}]^{7-}$, respectively, as they were those with features of fully reversibility. Preliminary single-point calculations indicated that the ground-state electronic configuration of the two compounds is best described with doublet multiplicity. We also optimized the molecular structure of the parent hexaanion, so to conduct a significative comparative analysis among the three isomers. The computed $[Rh_{16}Au_6(CO)_{36}]^{6-}$ structure is in good agreement with the single-crystal X-ray data. The root mean square deviation (RMSD) with respect to the experimental geometry is 0.296 Å (0.172 Å for what concerns the Au_6Rh_{16} core). The computed stationary points of the three $[Rh_{16}Au_6(CO)_{36}]^{n-}$ (n = 5, 6, 7) clusters are very similar, the RMSD between the parent hexaanion and the oxidized and the reduced species being 0.062 and 0.149 Å, respectively. The relative disposition of the metal atoms and the coordination modes of the ancillary ligands appear thus unaffected by the change of global charge. The average computed metal-metal bond lengths, summarized in Table 3, confirm the negligible variations in the metal cage.

Such a result is possibly to be ascribed to the widely delocalized nature of the frontier orbitals of $[Rh_{16}Au_6(CO)_{36}]^{6-}$,

Table 3. Computed average metal-metal bond lengths (Å) for $[Rh_{16}Au_6(CO)_{36}]^{n-}$ clusters.

Bond Lengths (Å)	$[Rh_{16}Au_6(CO)_{36}]^{7-}$	$[Rh_{16}Au_6(CO)_{36}]^{6-}$	$[Rh_{16}Au_6(CO)_{36}]^{5-}$
Au–Au	2.958	2.939	2.960
Au–Rh	2.874	2.852	2.835
Rh–Rh	2.856	2.846	2.838

Research Article
doi.org/10.1002/ejic.202400526

depicted in Figure 9. The sums of the Hirshfeld contributions[37] of the Au and Rh centres to the HOMO are respectively 24.6% and 35.7%. In the case of the LUMO the participation of the Rh centres is more important, 59.1%, while that of the Au atoms is lower, 11.2%.

The effects of the change of global charge on the metal-metal bonds were further investigated by means of the Atoms-in-Molecules (AIM) analysis. (3,–1) bond critical points (BCPs) are localized about in the middle of each Au–Au and Au–Rh couple when the distances between the metal centres are below 3.1 Å. In the cases of the Au–Rh interactions the BCPs are slightly closer to the Rh atoms, an effect attributable to the higher electronegativity of Au compared to Rh.[38] The Au_6Rh_{16} core of $[Rh_{16}Au_6(CO)_{36}]^{6-}$ with the Au–Au and Au–Rh BCPs is shown as example in Figure S1m. The negative values of energy density (E) and the positive values of the Laplacian of electron density ($\nabla^2\rho$) are in line with Bianchi's definition of metal-metal bond.[39] BCPs were instead not localized between the interacting Rh atoms, replaced by BCPs involving the μ-CO ligands.

The average values of electron density (ρ) and potential energy density (V) at Au–Au and Au–Rh BCPs, collected in Table S1b, indicate scarce influence of the variation of global cluster charge on the localized metal-metal bonds. Almost negligible changes were also observed for the properties computed at the (3,+3) cage critical points (CCPs) localized at about the centres of the Au_6 and Rh_4Au_2 octahedra (Table S1b and Figure S1m). The AIM data are thus in agreement with the previously described comparable structural features among the clusters computationally investigated.

Despite the similarities with the parent diamagnetic $[Rh_{16}Au_6(CO)_{36}]^{6-}$ anion, including the approximate D_{4h} symmetry of the Au_6Rh_{16} core, less pronounced for $[Rh_{16}Au_6(CO)_{36}]^{7-}$, the unpaired electron density derived from the monoelectronic oxidation or reduction of $[Rh_{16}Au_6(CO)_{36}]^{6-}$ is not uniformly distributed in the final clusters, as observable in Figure 10. The spin density of $[Rh_{16}Au_6(CO)_{36}]^{5-}$ is mainly localized on the central Au_6 fragment and on two Rh_4Au_2 octahedra in *trans* position with respect to the centre of the cluster. On the other hand, the spin density surface of $[Rh_{16}Au_6(CO)_{36}]^{7-}$ is mostly present on two mutually *cis* Rh_4Au_2 fragments.

Such an outcome is confirmed by the Löwdin spin population analysis. The values obtained for the atoms composing the metal cores, reported in Figure S1n, reveal that in the case of $[Rh_{16}Au_6(CO)_{36}]^{5-}$ the spin population is distributed with C_i symmetry. The spin population values are the same on comparing the Rh_4Au_2 octahedra in *trans* position, while mutually *cis* Rh_4Au_2 octahedra have different spin populations. The values are much less symmetric for $[Rh_{16}Au_6(CO)_{36}]^{7-}$. Two Rh_4Au_2 octahedra in *cis* position have quite high spin population, while the spin values for the other atoms composing the metal core are close to zero.

Experimental Section

General procedures. All reactions were performed using standard Schlenk technique under either N_2 or CO. Solvents were dried and degassed before use; tetrahydrofuran (THF) was dehydrated with sodium benzophenone and distilled under nitrogen. IR spectra were recorded on a PerkinElmer Spectrum One interferometer in CaF_2 cells. Positive/negative-ion mass spectra were recorded in CH_3CN solutions on a Waters Micromass ZQ 4000 using electrospray ionization. Experimental conditions: 2.56 kV ES-probe voltage, 10 V cone potential, 250 L/h flow of N_2 spray-gas, incoming solution flow 20 μL min^{-1}.

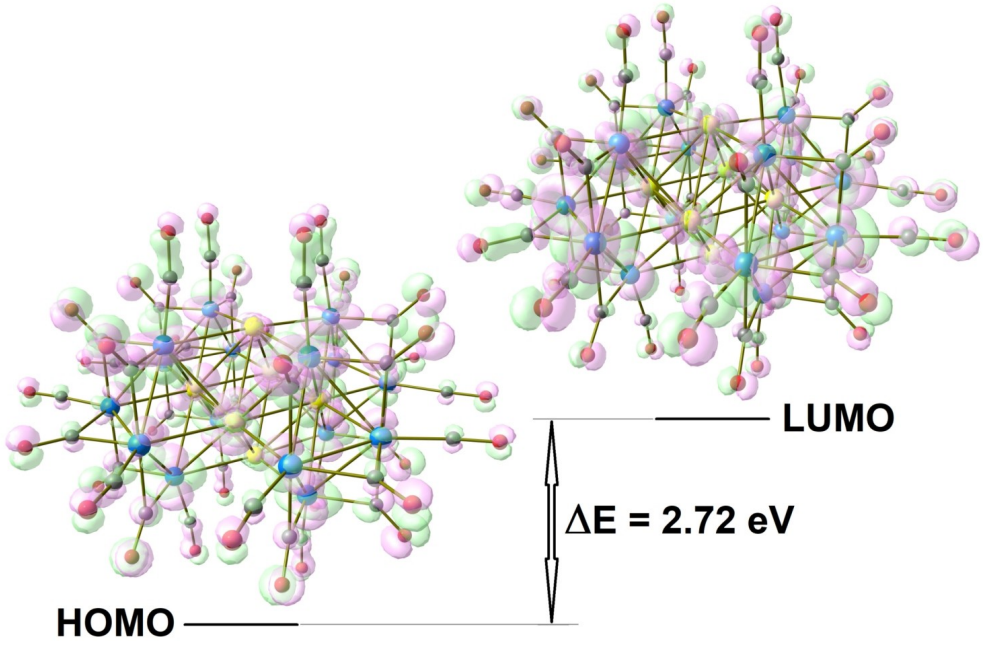

Figure 9. DFT-optimized structure of $[Rh_{16}Au_6(CO)_{36}]^{6-}$ with plots of the frontier molecular orbitals (green and pink tones, surface isovalue = 0.03 a.u.) and HOMO-LUMO gap. Rh atoms are in blue, Au atoms in yellow, C atoms in grey, O atoms in red.

Research Article
doi.org/10.1002/ejic.202400526

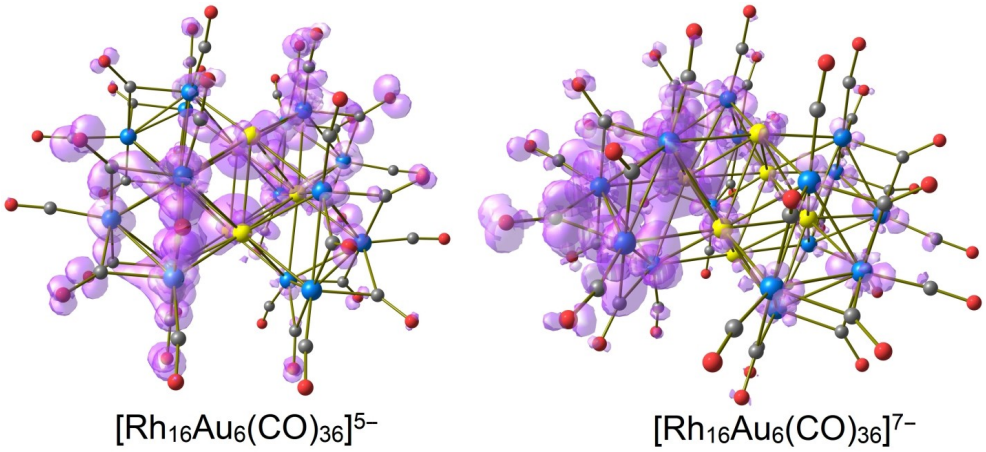

Figure 10. DFT-optimized structures of $[Rh_{16}Au_6(CO)_{36}]^{5-}$ and $[Rh_{16}Au_6(CO)_{36}]^{7-}$ with plots of the spin density (violet tones, surface isovalue = 0.001 a.u.). Rh atoms are in blue, Au atoms in yellow, C atoms in grey, O atoms in red.

Electrochemical Experiments

Materials and apparatus for electrochemistry and IR SEC have been described elsewhere.[40] CV and IR SEC measurements were performed on CO-saturated CH_3CN/[TBA]PF_6 0.1 M solutions of $[Rh_{16}Au_6(CO)_{36}][TEA]_6$ (1.2 ÷ 1.5 mM). Glassy-carbon electrodes, used as working electrodes for the voltammetric experiments, were polished, prior to measurements, according to the following procedure: manual rubbing with 0.3 μm Al_2O_3 slurry in water (eDAQ) for 2 min, then sonication in ultrapure water for 10 min, manual rubbing with 0.05 μm Al_2O_3 slurry in water (eDAQ) for 2 min, then sonication in ultrapure water for 10 min. After polishing, the electrodes were rinsed with acetone and air-dried. A leakless miniature Ag/AgCl/KCl electrode (eDAQ) was employed as a reference. Under the present experimental conditions, the one-electron oxidation of ferrocene occurs at $E^\circ = +0.42$ V vs. Ag/AgCl.

Molecular Structure Determination

Single-crystal X-ray diffraction analysis of cluster **2** was performed at 100 K with a Bruker Apex II diffractometer, equipped with a CMOS detector, by using Kα-Mo radiation. Data were corrected for Lorentz polarization and absorption effects (empirical absorption correction SADABS).[41] After the absorption correction, due to the presence of heavy atoms like both Rh and Au, some high residual density close to them, the highest closer to the Au atom, still remained and could not be eliminated. Considering their proximity to the heavy metals, we can confidently state that they do not correspond to any undefined atom. The structure was solved by direct methods and refined by full-matrix least-squares based on all data using F^2.[42] Hydrogen atoms belonging to the $TBMA^+$ cations were fixed at calculated positions and refined by a riding model. All non-hydrogen atoms were refined with anisotropic displacement parameters. Molecular structures were drawn with SCHAKAL99.[43]

Computational Details

Geometry optimizations were carried out using the PBEh-3c method, which is a reparametrized version of PBE (with 42% HF exchange)[44] that uses a split-valence double-zeta basis set (def2-mSVP) with relativistic effective core potentials accounting for 28 electrons of the Rh atoms and 60 electrons of the Au atoms.[45] The method adds three corrections considering dispersion, basis set superposition, and other basis set incompleteness effects.[46] In the case of an odd number of electrons, the lack of spin contamination was verified by comparing the computed $< S^2 >$ values with the theoretical ones. The software used was ORCA version 5.0.3.[47] The output was elaborated using MultiWFN, version 3.8.[48] Cartesian coordinates of the DFT-optimized structures are collected in a supplementary Coordinates RhAu.xyz file.

Synthesis of $[Rh_{16}Au_6(CO)_{36}]^{6-}$ (1)

A THF solution of $[AuCl_4][TEA]$ (0.15 g, 0.32 mmol) was added dropwise to a solution containing $[Rh_7(CO)_{16}][TBA]_3$ (0.60 g, 0.32 mmol) in the same solvent under carbon monoxide atmosphere. The solution was left under vigorous stirring overnight. The formed precipitate was separated from the solution through filtration. The solid was washed with THF, then dichloromethane and dissolved in acetonitrile. By layering a small amount of hexane and di-isopropyl ether onto the solution, crystals of $[Rh_{16}Au_6(CO)_{36}][TEA]_6$ were obtained (yield around 35% based on Rh). The salt is fairly soluble in acetone, soluble in acetonitrile and DMF and stable, but not soluble, in water. The IR spectrum of **1**$[TEA]_6$ recorded in acetonitrile shows ν_{CO} absorptions at 2006(s), 1981(ms) and 1802(m) cm^{-1}. ESI-MS analysis of **1**$[TEA]_6$ was carried out in acetonitrile and the spectrum of the negative region shows two main groups of peaks related to z = 2 and z = 3. In the first group it is possible to detect the $[Rh_{16}Au_6(CO)_{27}]^{2-}$ ion at 1792 m/z. In this same area there are signals due to the cluster where either one or two TEA^+ counterions are retained, more specifically at 1871 and 1992 m/z, related to the $\{[Rh_{16}Au_6(CO)_{28}][TEA]\}^{2-}$ and $\{[Rh_{16}Au_6(CO)_{32}][TEA]_2\}^{2-}$ ions, respectively. In the second group it is possible to observe signals at 1213 and 1266 m/z corresponding to the $[Rh_{16}Au_6(CO)_{29}]^{3-}$ and $\{[Rh_{16}Au_6(CO)_{30}][TEA]\}^{3-}$ ions, respectively. Each of the aforementioned peaks was accompanied by others deriving from subsequent CO loss.

Synthesis of $[Rh_{10}Au(CO)_{26}]^{3-}$ (2).

A DMF solution of $[AuCl_4][TEA]$ (0.20 g, 0.43 mmol) was slowly added to a solution of $[Rh_7(CO)_{16}][TEA]_3$ (0.67 g, 0.43 mmol) in the same solvent, under CO atmosphere, and in a 1:1 molar ratio. After being left under stirring overnight, the resulting solution was precipitated with an aqueous solution of TEACl and the solid washed with water, ethanol and THF. The residue was extracted with acetone, then a metathesis with an aqueous solution of

Research Article
doi.org/10.1002/ejic.202400526

TBMACl was performed. The solid was re-dissolved in acetone and layered with hexane; after a few days, crystals of **2**[TBMA]$_3$ were obtained (yield around 50% based on Rh). [$Rh_{10}Au(CO)_{26}$][TBMA]$_3$ is soluble in acetone, acetonitrile and DMF and stable, but not soluble, in water. The IR spectrum of **2**[TBMA]$_3$ recorded in CH_3CN shows ν_{CO} absorptions at 2040(m), 2010(vs), 1828(m), 1803(m) and 1772(mw) cm^{-1}. ESI-MS analysis of [$Rh_{10}Au(CO)_{26}$][TBMA]$_3$ in CH_3CN shows, in the negative region, two main groups of signals plus a single low-intensity one at 968 m/z, which can be assigned to the {[$Rh_{10}Au(CO)_{20}$][TBMA]}$^{2-}$ ion. The first group starts at 907 m/z and is attributable to the [$Rh_{10}Au(CO)_{21}$]$^{2-}$ ion accompanied by signals due to CO loss (893, 879, 865, 851, 837, 822, 808 and 794 m/z for the [$Rh_{10}Au(CO)_{20\text{-}19\text{-}18\text{-}17\text{-}16\text{-}15\text{-}14\text{-}13}$]$^{2-}$ ions, respectively). The second group of peaks indicates the cluster fragmentation, since it starts at 510 m/z, corresponding to the [$Rh_5Au(CO)_{11}$]$^{2-}$ ion, with progressive losses of CO ligands up to 454 m/z.

Conclusions

In this paper we presented the optimization of the synthesis of the previously reported atomically-precise [$Rh_{16}Au_6(CO)_{36}$]$^{6-}$ (**1**) nanocluster, by performing a thorough reaction screening varying various parameters like solvent, stoichiometric ratio, counterion and atmosphere (either N_2 or CO). From the obtained results the first conclusion is that the CO atmosphere (with a pressure around 1.5 atm) is necessary to obtain heterometallic Rh–Au clusters, whereas by conducting the reaction under N_2 only homometallic rhodium species were identified. Furthermore, one key parameter to reach a higher selectivity of **1** is its solubility, or rather lack thereof, in the reaction medium, which was attained by finding the right combination of solvent and positive counterion, namely THF and TBA^+/TEA^+. This way cluster **1**, once formed, is subtracted from the mother solution by its precipitation as TEA^+ salt, and this prevents the cluster from undergoing further reactions. A proof of this is that by carrying out the reaction in a homogeneous environment, its formation is lowered by the concurrent formation of **2**, which appears to be deriving from the oxidation of **1**.

The obtaining of **1** in fairly good amount allowed the completion of its characterization via IR spectroscopy and ESI-MS. Furthermore, its remarkable electron-sponge behaviour was unravelled by electrochemical and spectroelectrochemical experiments, as [$Rh_{16}Au_6(CO)_{36}$]$^{n-}$ is capable to exist in four long-lived differently charged states in addition to the initial one, namely n = 5, 6, 7, 9, 10, and still retaining its molecular structure. The presence of a sixth charged state with n = 8 was suggested by the analysis of the IR sequence registered over the SEC experiments, and its IR spectrum was derived from a spectral deconvolution taking into considerations the different contributions to its original pattern. DFT calculations supported the fully reversible electrochemical formation of paramagnetic [$Rh_{16}Au_6(CO)_{36}$]$^{5-}$ and [$Rh_{16}Au_6(CO)_{36}$]$^{7-}$ clusters, characterized by very similar geometries and Au–M bond strengths with respect to the parent [$Rh_{16}Au_6(CO)_{36}$]$^{6-}$ hexaanion.

The in-depth investigation of the synthesis of **1** also allowed the isolation and characterization of a new atomically-precise heterometallic nanocluster, namely [$Rh_{10}Au(CO)_{26}$]$^{3-}$ (**2**), whose dimensions of length and width are of about 1.4 and 1.0 nm, respectively. Cluster **2** was unambiguously identified by SC-XRD analysis and characterized by IR spectroscopy and ESI mass-spectrometry. Remarkably, its octahedral-based structural motif can also be observed in **1** and in the even larger [$Ni_{32}Au_6(CO)_{44}$]$^{6-}$ nanocluster. Both octahedral-based structures in cluster **1** and **2** were somewhat surprising when compared with those of other heterometallic Rh nanoclusters, like the [$Rh_{12}E(CO)_{27}$]$^{n-}$ series of compounds (E=Ge, Sn, Sb, Bi; n = 4, 3) and most of their derivatives,[6] which all have an icosahedral-based geometry. Gold homometallic clusters too often show a preference for the latter architecture.[49] However, the geometrical versatility of carbonyl metal nanoclusters is well known, as it is the result of the best combination of various factors like the metal-metal and metal-ligand bond strengths, steric hindrance and the fulfilling of electronic requirements.

Ultimately, the present study allowed to disclose a very complex Rh–Au chemical system which can give rise to new nanoclusters, some of which we were able to only partially identify, and that will be further investigated in the future.

Funding

The work was funded by PRIN 2022: "COntrolled Shuttling inside artificial MOlecular tubes" (COSMO) – Code 20227JMTLE, CUP J53D23008520006 by Ministero dell'Università e della Ricerca (MUR); by NEST–Network 4 Energy Sustainable Transition Spoke 9: Energy-Sustainable Advanced Materials, Code PE0000021, CUP J33C22002890007 Concession Decree No. 1561 of 11 October 2022 by (MUR); and by the University of Bologna.

Acknowledgements

Authors wish to acknowledge Mr. Luca Zuppiroli for the ESI-MS experiments, and Dr Sara Khaliha for her early work on this topic during her bachelor thesis. Open Access publishing facilitated by Università degli Studi di Bologna, as part of the Wiley - CRUI-CARE agreement.

Conflict of Interests

The authors declare no conflict of interest.

Data Availability Statement

The data that support the findings of this study are available in the supplementary material of this article.

Keywords: Rhodium · Gold · X-ray diffraction · Electrochemistry · DFT

[1] a) M. Zhou, C. Zeng, Y. Chen, S. Zhao, M. Y. Sfeir, M. Zhu, R. Jin, *Nat. Commun.* **2016**, *7*, 13240; b) I. Russier-Antoine, F. Bertorelle, M. Vojkovic, D. Rayane, E. Salmon, C. Jonin, P. Dugourd, R. Antoine, P.-F. Brevet, *Nanoscale* **2014**, *6*, 13572–13578.
[2] a) S. Zhu, X. Wang, Y. Cong, L. Li, *ACS Omega* **2020**, *5*, 22702–22707; b) X. Qu, Y. Li, L. Li, Y. Wang, J. Liang, J. Liang, *J. Nanomater.* **2015**, *2015*, 784097.
[3] P. Buchwalter, J. Rosé, P. Braunstein, *Chem. Rev.* **2015**, *115*, 28–126.
[4] B. K. Teo, X. Shi, H. Zhang, *J. Am. Chem. Soc.* **1991**, *113*, 4329–4331.
[5] a) Y. Wang, C. G. Gianopoulos, Z. Liu, K. Kirschbaum, D. Alfonso, D. R. Kauffman, R. Jin, *JACS Au* **2024**, *4*, 1928–1934; b) V. Truttmann, A. Loxha, R. Banu, E. Pittenauer, S. Malola, M. F. Matus, Y. Wang, E. A. Ploetz, G. Rupprechter, T. Bürgi, H. Häkkinen, C. Aikens, N. Barrabés, *ACS Nano* **2023**, *17*, 20376–20386; c) Q. Yao, L. Liu, S. Malola, M. Ge, H. Xu, Z. Wu, T. Chen, Y. Cao, M. F. Matus, A. Pihlajamäki, Y. Han, H. Häkkinen, J. Xie, *Nat. Chem.* **2023**, *15*, 230–239.
[6] G. Bussoli, C. Cesari, C. Femoni, M. C. Iapalucci, S. Ruggieri, S. Zacchini *in Atomically Precise Nanochemistry*, Editor(s): Rongchao Jin, De-en Jiang, © John Wiley & Sons Ltd., **2023**, *Chapter 10*, pp. 309–330, 10.1002/9781119788676.ch10. Print ISBN: 9781119788645 Online ISBN: 9781119788676.
[7] C. Femoni, C. Cesari, M. C. Iapalucci, S. Ruggieri, S. Zacchini, *in Comprehensive Organometallic Chemistry IV* (ed. G. Parkin, K. Meyer, D. O'Hare) Elsevier **2022**, 205–270, doi.org/10.1016/B978-0-12-820206-7.00151-7 (chapter). ISBN 9780323913508 (book).
[8] M. Joost, L. Estévez, S. Mallet-Ladeira, K. Miqueu, A. Amgoune, D. Bourissou, *Angew. Chem. Int. Ed.* **2014**, *53*, 14512–14516.
[9] G. Bistoni, S. Rampino, N. Scafuri, G. Ciancaleoni, D. Zuccaccia, L. Belpassi, F. Tarantelli, *Chem. Sci.* **2016**, *7*, 1174–1184.
[10] I. Ciabatti, C. Femoni, M. C. Iapalucci, S. Ruggieri, S. Zacchini, *Coord. Chem. Rev.* **2018**, *355*, 27–38.
[11] a) L. Cerchi, A. Fumagalli, S. Fedi, P. Zanello, F. Fabrizi De Biani, F. Laschi, L. Garlaschelli, P. Macchi, A. Sironi, *Inorg. Chem.* **2012**, *51*, 9171–9180; b) M. Bortoluzzi, I. Ciabatti, C. Femoni, M. Hayatifar, M. C. Iapalucci, G. Longoni, S. Zacchini, *Dalton Trans.* **2014**, *43*, 13471–13475; c) A. Ceriotti, P. Macchi, A. Sironi, S. El Afefey, M. Daghetta, S. Fedi, F. Fabrizi De Biani, R. Della Pergola, *Inorg. Chem.* **2013**, *52*, 1960–1964; d) R. D. Adams, Y. Kan, Q. Zhang, *Organometallics* **2012**, *31*, 8639–8646.
[12] a) N. T. Tran, M. Kawano, D. R. Powell, R. K. Hayashi, C. F. Campana, L. F. Dahl, *J. Am. Chem. Soc.* **1999**, *121*, 5945–5952; b) E. G. Mednikov, L. F. Dahl, *Inorg. Chem.* **2015**, *54*, 1145–1151; c) C. Femoni, M. C. Iapalucci, G. Longoni, C. Tiozzo, S. Zacchini, *Angew. Chem. Int. Ed.* **2008**, *47*, 6666–6669; d) P. Croizat, S. Sculfort, R. Welter, P. Braunstein, *Organometallics* **2016**, *35*, 3949–3958; e) S. R. Drake, K. Henrick, B. F. G. Johnson, J. Lewis, M. McPartlin, J. Morris, *J. Chem. Soc., Chem. Commun.* **1986**, 928–930.
[13] a) W. O. Hieber, E. H. Schubert, *Z. Anorg. Allg. Chem.* **1965**, *338*, 32–36; b) P. Chini, *J. Organomet. Chem.* **1980**, *200*, 37–61.
[14] a) I. Ciabatti, F. Fabrizi de Biani, C. Femoni, M. C. Iapalucci, G. Longoni, S. Zacchini, *ChemPlusChem* **2013**, *78*, 1456–1465; b) C. Femoni, M. C. Iapalucci, G. Longoni, P. H. Svensson, J. Wolowska, *Angew. Chem. Int. Ed.* **2000**, *39*, 1635–1637.
[15] C. Capacci, C. Cesari, C. Femoni, M. C. Iapalucci, F. Mancini, S. Ruggieri, S. Zacchini, *Inorg. Chem.* **2020**, *59*, 16016–16026.
[16] C. Femoni, M. C. Iapalucci, S. Ruggieri, S. Zacchini, *Acc. Chem. Res.* **2018**, *51*, 2748–2755.
[17] S. Martinengo, P. Chini, *Gazz. Chim. Ital.* **1972**, *102*, 344–354.
[18] C. Femoni, T. Funaioli, M. C. Iapalucci, S. Ruggieri, S. Zacchini, *Inorg. Chem.* **2020**, *59*, 4300–4310.
[19] A. Fumagalli, S. Martinengo, G. Ciani, A. Sironi, *J. Chem. Soc., Chem. Commun.* **1983**, 453–455.
[20] P. Chini, S. Martinengo, *Inorg. Chim. Acta* **1969**, *3*, 299–302.
[21] D. Collini, F. Fabrizi De Biani, S. Fedi, C. Femoni, F. Kaswalder, M. C. Iapalucci, G. Longoni, C. Tiozzo, S. Zacchini, P. Zanello, *Inorg. Chem.* **2007**, *46*, 7971–7981.
[22] A. Fumagalli, T. F. Koetzle, F. Takusagawa, P. Chini, S. Martinengo, B. T. Heaton, *J. Am. Chem. Soc.* **1980**, *102*, 1740–1742.
[23] a) K. Wade, *Inorg. Nucl. Chem. Lett.* **1978**, *14*, 71–74; b) A. K. Hughes, K. Wade, *Coord. Chem. Rev.* **2000**, *197*, 191–229.
[24] Deposition number 2375461 contains the supplementary crystallographic data for this paper (cluster **2**). Deposition number 1861421 contains the supplementary crystallographic data for cluster **1**. These data are provided free of charge by the joint Cambridge Crystallographic Data Centre and Fachinformationszentrum Karlsruhe Access Structures service.
[25] a) I. Ciabatti, C. Femoni, M. C. Iapalucci, G. Longoni, S. Zacchini, S. Fedi, F. Fabrizi De Biani, *Inorg. Chem.* **2012**, *51*, 11753–11761; b) B. F. G. Johnson, D. A. Kaner, J. Lewis, P. R. Raithby, *J. Chem. Soc., Chem. Commun.* **1981**, 753–755.
[26] M. Bortoluzzi, I. Ciabatti, C. Femoni, T. Funaioli, M. Hayatifar, M. C. Iapalucci, G. Longoni, S. Zacchini, *Dalton Trans.* **2014**, *43*, 9633–9646.
[27] M. F. Hallam, D. M. P. Mingos, T. Adatia, M. McPartlin, *J. Chem. Soc., Dalton Trans.* **1988**, 335–340.
[28] N. de Silva, J. W. Laufenberg, L. F. Dahl, *Chem. Commun.* **2006**, 4437–4439.
[29] B. F. G. Johnson, D. A. Kaner, J. Lewis, P. R. Raithby, *J. Chem. Soc., Chem. Commun.* **1981**, 753–755.
[30] C. Femoni, M. C. Iapalucci, G. Longoni, C. Tiozzo, J. Wolowska, S. Zacchini, E. Zazzaroni, *Chem. Eur. J.* **2007**, *13*, 6544–6554.
[31] P. Braunstein, J. Rosé, A. Tiripicchio, M. Tiripicchio Camellini, *Angew. Chem. Int. Ed.* **1985**, *24*, 767–768.
[32] C. Cesari, M. Bortoluzzi, C. Femoni, M. C. Iapalucci, S. Zacchini, *Inorg. Chim. Acta* **2023**, *545*, 121281.
[33] T. Nakajima, A. Ishiguro, Y. Wakatsuki, *Angew. Chem. Int. Ed.* **2001**, *40*, 1066–1068.
[34] M. Krejčik, M. Daněk, F. Hartl, *J. Electroanal. Chem. Interfacial Electrochem.* **1991**, *317*, 179–187.
[35] a) J. D. Roth, G. J. Lewis, L. K. Safford, X. Jiang, L. F. Dahl, M. J. Weaver, *J. Am. Chem. Soc.* **1992**, *114*, 6159–6169; b) C. Cesari, B. Berti, M. Bortoluzzi, C. Femoni, T. Funaioli, F. M. Vivaldi, M. C. Iapalucci, S. Zacchini, *Dalton Trans.* **2023**, *52*, 3623–3642.
[36] M. E. Prater, L. E. Pence, R. Clérac, G. M. Finniss, C. Campana, P. Auban-Senzier, D. Jérome, E. Canadell, K. R. Dunbar, *J. Am. Chem. Soc.* **1999**, *121*, 8005–8016.
[37] T. Lu, F. Chen, *Acta Chim. Sin.* **2011**, *69*, 2393–2406.
[38] C. Tantardini, A. R. Oganov, *Nat. Commun.* **2021**, *12*, 2087.
[39] C. Lepetit, P. Fau, K. Fajerwerg, M. L. Kahn, B. Silvi, *Coord. Chem. Rev.* **2017**, *345*, 150–181.
[40] B. Berti, C. Cesari, C. Femoni, T. Funaioli, M. C. Iapalucci, S. Zacchini, *Dalton Trans.* **2020**, *49*, 5513–5522.
[41] G. M. Sheldrick, *SADABS, Program for Empirical Absorption Correction*, University of Göttingen, Germany **1996**.
[42] G. M. Sheldrick, *SHELX 2014/7, Program for Crystal Structure Determination*, University of Göttingen, Germany **2014**.
[43] E. Keller, *SCHAKAL99*, University of Freiburg, Germany **1999**.
[44] a) S. Grimme, J. G. Brandenburg, C. Bannwarth, A. Hansen, *J. Chem. Phys.* **2015**, *143*, 054107; b) A. A. Otlyotov, A. D. Moshchenkov, L. Cavallo, Y. Minenkov, *Phys. Chem. Chem. Phys.* **2022**, *24*, 17314–17322.
[45] a) F. Weigend, R. Ahlrichs, *Phys. Chem. Chem. Phys.* **2005**, *7*, 3297–3305; b) F. Weigend, *Phys. Chem. Chem. Phys.* **2006**, *8*, 1057–1065.
[46] a) H. Kruse, S. Grimme, *J. Chem. Phys.* **2012**, *136*, 154101; b) S. Grimme, S. Ehrlich, L. Goerigk, *J. Comput. Chem.* **2011**, *32*, 1456–1465; c) S. Grimme, J. Antony, S. Ehrlich, H. Krieg, *J. Chem. Phys.* **2010**, *132*, 154104.
[47] F. Neese, *Wiley Interdiscip. Rev.: Comput. Mol. Sci.* **2022**, *12*, e1616.
[48] T. Lu, F. Chen, *J. Comput. Chem.* **2012**, *33*, 580–592.
[49] C. Zeng, Y. Chen, K. Kirschbaum, K. Appavoo, M. Y. Sfeir, R. Jin, *Sci. Adv.* **2015**, *1*, e1500045.

Manuscript received: August 13, 2024
Revised manuscript received: September 30, 2024
Accepted manuscript online: November 2, 2024
Version of record online: November 16, 2024